New systematic features in the neutron-deficient Au isotopes

OPEN ACCESS
IOP Publishing

Made open access 12 September 2017
Journal of Physics G: Nuclear and Particle Physics

J. Phys. G: Nucl. Part. Phys. **44** (2017) 074003 (20pp) https://doi.org/10.1088/1361-6471/aa7297

New systematic features in the neutron-deficient Au isotopes*

M Venhart[1], J L Wood[2], M Sedlák[1], M Balogh[1], M Bírová[1], A J Boston[3], T E Cocolios[4,5], L J Harkness-Brennan[3], R-D Herzberg[3], L Holub[1], D T Joss[3], D S Judson[3], J Kliman[1], J Klimo[1], L Krupa[1,6], J Lušnák[1,9], L Makhathini[7], V Matoušek[1], Š Motyčák[6,8], R D Page[3], A Patel[3], K Petrík[1], A V Podshibyakin[6], P M Prajapati[1], A M Rodin[6], A Špaček[1], R Urban[1], C Unsworth[3] and M Veselský[1]

[1] Institute of Physics, Slovak Academy of Sciences, SK-84511 Bratislava, Slovakia
[2] Department of Physics, Georgia Institute of Technology, Atlanta, GA 30332, United States of America
[3] Department of Physics, Oliver Lodge Laboratory, University of Liverpool, Liverpool, L69 7ZE, United Kingdom
[4] School of Physics and Astronomy, The University of Manchester, Manchester M13 9PL, United Kingdom
[5] KU Leuven, Instituut voor Kern- en Stralingsfysica, B-3001 Leuven, Belgium
[6] Flerov Laboratory of Nuclear Reactions, JINR, RU-141 980, Dubna, Russia
[7] iThemba Laboratory for Accelerator Based Sciences, PO Box 722, 7129 Somerset West, South Africa
[8] Faculty of Electrical Engineering and Information Technology, Slovak University of Technology, SK-812 19 Bratislava, Slovakia

E-mail: martin.venhart@savba.sk

Received 31 October 2016, revised 27 April 2017
Accepted for publication 11 May 2017
Published 8 June 2017

Abstract

A recently developed portable, on-line capability for γ-ray and conversion-electron spectroscopy, HIGH-TATRA is demonstrated with its application to the study of ^{183}Hg $\rightarrow$ ^{183}Au at ISOLDE. Key details of the low-energy level scheme of the neutron-deficient nuclide ^{183}Au populated in this decay are presented. A broad energy germanium detector is employed to achieve this (the first-ever use of such a device in decay-scheme spectroscopy), by way of a combination of high-gain γ-ray singles spectroscopy and γ–γ coincidence spectroscopy. Further, by combining the γ-ray detectors with a liquid-nitrogen-cooled Si(Li) detector operated under high vacuum, conversion-electron singles and e–γ coincidences are obtained. These data

* This article belongs to the Focus on Exotic Beams at ISOLDE: A Laboratory Portrait special issue.
[9] Student of Secondary School of Electrical Engineering, K. Adlera 5, Bratislava, Slovakia.

lead to the determination of transition multipolarities and the location of a highly converted ($E0 + M1 + E2$) transition in the ^{183}Au decay scheme, suggesting a possible new shape coexisting structure in this nucleus. Identification of new intruder and normal states fixes their relative energies in ^{183}Au for the first time. New systematic features in the odd-Au isotopes are presented.

Keywords: nuclear structure, broad energy germanium detector, conversion electrons, HIGH-TATRA spectrometer, shape coexistence

(Some figures may appear in colour only in the online journal)

1. Introduction

A major strategic theme that has been overarching to the study of nuclear structure far from stability is the elucidation of systematic features of selected properties of nuclei: masses; charge radii; properties of the first few excited states; properties of states with specified spin-parity. One particular feature of nuclei whose observation has depended heavily on systematic study is the phenomenon of shape coexistence in nuclei. Three major reviews [1–3] and a focus issue [4] have documented this evolution.

In the present account we give details of an on-going quest to elucidate the nature of shape coexistence in the neutron deficient Pt, Au, Hg, Tl, Pb, Bi, Po region with special focus on the odd-mass Au isotopes. This particularly addresses the complex spectroscopy involved.

2. Shape coexistence in the neutron-deficient Au isotopes and their neighbours

An interest in systematic study of the Au isotopes can be traced back to before the emergence of shape coexistence as a feature of heavy nuclei. Experiments at the UNISOR [5] and the ISOCELE facilities [6, 7] revealed a remarkable constancy in excitation energies for many low-lying excited states in the odd-Au isotopes. However, 'intruder' states, i.e., 'unexpected' states that appeared at low energy, were established in the most neutron-deficient Au isotopes accessible at the time [6, 7]. This led to the first review of shape coexistence in nuclei [1].

The structure of the neutron-deficient Au isotopes became clearer with the summary provided in a paper by Kortelahti *et al* in 1988 [8]. We direct the reader to this paper for a detailed perspective on the structures expected in ^{183}Au. It revealed a complex situation of four coexisting structures in ^{185,187}Au. A very detailed investigation of the decays of ^{187}Hg^{m,g} to ^{187}Au followed [9–11]. A more limited study of the decays of ^{185}Hg^{m,g} to ^{185}Au was also carried out [12, 13]. These studies involved measurements of conversion electrons using e–γ coincidences and identification of electric monopole transitions ($E0$), which provide a model-independent fingerprint of shape coexistence [14, 15]. However, a full understanding of the detailed structure was lacking. An investigation of the decay of ^{183}Hg to ^{183}Au [16] implied that limitations of source intensity, combined with extreme complexity, had to be overcome for studies of the neutron-deficient Au isotopes to continue. While some in-beam γ-ray spectroscopy studies of even more neutron deficient Au isotopes [17–26] were carried out following the radioactive decay programme, only information on yrast structures was obtained. These data supported the interpretation in terms of collective bands built on intruder states, but in most cases were unable to determine the excitation energies of the band heads.

In figure 1 we present a systematic view of the current information of the neutron-deficient Au isotopes. It particularly shows the parabolic trend of the intruder states due to the $1h_{9/2}$ configuration. A critical step in establishing this view was the discovery of a low-spin

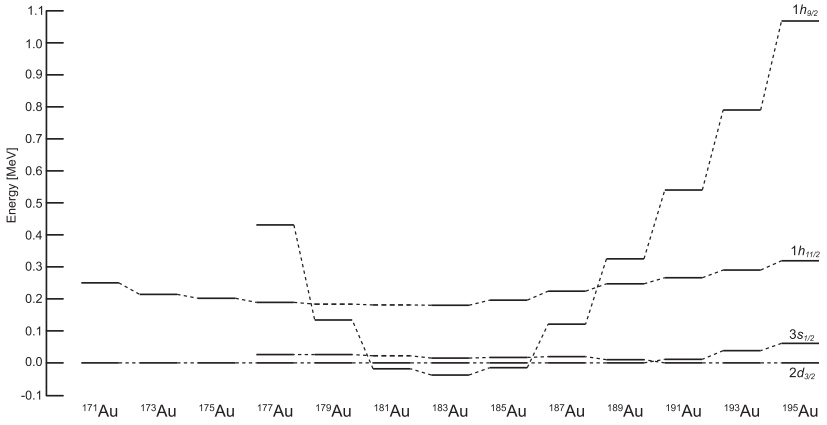

Figure 1. Systematics of $3s_{1/2}$, $2d_{3/2}$, $1h_{11/2}$ and $1h_{9/2}$ proton configurations in neutron-deficient odd-Au isotopes. The data are taken from [5, 8, 11, 13, 16, 26–28].

microsecond isomer in ^{179}Au [28]: the combination of population by in-beam γ-ray spectroscopy and delayed decays, combined with α-decay information and mass measurements was critical in arriving at a unique interpretation of these data. While figure 1 provides a basic view of the intruder state dominance of the low-lying states near $N = 104$ (mid-neutron shell), it is incomplete with respect to the multiple coexisting structures established in ^{185,187}Au [11, 13].

The challenge of elucidating the pattern of multiple coexisting structures in the Au isotopes (and, indeed, anticipated similar structures in other nuclei in this mass region) has led to a new spectroscopic initiative from the group at the Institute of Physics, Slovak Academy of Sciences in Bratislava, Slovakia. The construction of a dedicated conversion-electron detection system based on a liquid nitrogen cooled Si(Li) detector has been complemented by state-of-the-art broad energy germanium detectors (BEGe) [29] for γ-rays that are under investigation at the University of Liverpool. Conjunction of these techniques allowed the initiation of detailed studies of nuclear structure. This is motivated by evident failures in the study of ^{185}Au [12], which are identified below. In the following, we describe details of this initiative, which has now evolved through the successful commissioning of all key steps and is ready for detailed spectroscopic studies of odd-mass Au isotopes (and other nuclei with very complex level schemes).

3. Experimental details

The appearance of intruder states at very low energy in nuclei means that it is essential to characterise their behaviour in order to interpret decay scheme information. This is critical far from stability where systematics is often used to infer structure. However, it is these same states that lead to complexity in such decay schemes. Not only is the low-energy level density increased (approximately by a factor of 2), but intruder states exhibit isomerism [8, 28] which may result in isolated groups of transitions that are unconnected by prompt coincidence information. In some cases, the excitation energy of these isomers can be established using high-resolution mass spectrometry in a Penning trap [30]. Further, the very low excitation energy of these states often results in very low-energy transitions that are not easily observed and can be missed. In principle, energy differences and sums of γ-ray energies, i.e., the

Rydberg–Ritz combination principle [31], which was originally proposed to explain the relationship of atomic spectral lines, can resolve this problem, but the line density in γ-ray spectra is so high that ambiguities generally prevent this approach. It is important to identify doublets (or even higher multiplets) in a γ-ray spectrum. Missing them usually leads to misinterpretation of the data. In this work we use a technique which we have developed in [32] in conjunction with the presently reported study to make an advance in addressing this issue by the use (to our knowledge the first-ever in decay spectroscopy) of a modern BEGe [29] detector with high energy resolution over a broad energy range, operated at high gain and in coincidence mode.

Two separate experiments were performed at the ISOLDE facility at CERN. A pulsed beam of protons with an energy of 1.4 GeV and average intensity of 1.5 μA, which was delivered by the PS booster accelerator, impinged on a molten lead target inducing spallation, fission and fragmentation processes. Due to the high temperature of the target, reaction products diffused out of the target. They were ionised using a plasma ion source and extracted with a 30 kV potential. Since the Hf–Pt elements are refractory and thus are not released from the target, the production was essentially limited to Hg isotopes. After extraction from the ion source, the beam was separated employing the general purpose separator of the ISOLDE facility, which has one analysing magnet [33].

Mass-separated samples of the ^{183}Hg were created by a deposition of the radioactive-ion beam onto the tape of the TATRA transportation system [34]. After a collection period of 1s, samples were transported by rapid motion of the tape into the measurement position. The transportation time was approximately 0.8 s. The data were collected during 30 s period and then the process was periodically repeated. At the measurement position, an array of three hyper-pure germanium detectors was employed to detect the γ-rays following the β^+/EC decay of ^{183}Hg and its daughter products. In the first experiment, a BE2020 type BEGe detector was used to detect γ-rays in the 40–980 keV range. Two coaxial germanium detectors with relative efficiencies of 70% were used to detect γ-rays in the range 40–2500 keV. Gamma-rays below 40 keV could not be detected due to the 3 mm thick stainless steel wall of the TATRA system. Each detector was instrumented with an independent channel of the fully digital, triggerless data acquisition system. The stream of timestamped data was written to the disk. The time-gated and prompt coincidence spectra were reconstructed offline. Further details are given in [32].

Based on the experience gained in the first experiment, the TATRA system was modified to the HIGH-TATRA system. Transmission of low-energy γ-rays was improved by installation of 50 μm thick titanium windows at the measurement position. The γ-ray detection efficiency was increased by installation of a third coaxial germanium detector. A windowless Si(Li) detector, type SSL80155 produced by Canberra, with a thickness of 5 mm and surface area of 80 mm^2, operated at liquid nitrogen temperature, was used to detect conversion and Auger electrons, characteristic x-rays, and low-energy γ-rays. The vacuum inside of the system was improved with a differential pumping system, to avoid icing of the detector surface. During the experiment, the system was operated below 1.0×10^{-7} mbar. Icing of the detector surface (and thus deterioration of the electron peak shape) was not observed even after several days of exposure of the system to the inferior vacuum in the ISOLDE beam line. Conversion electrons with energies above 200 keV were detected with FWHM of 1.2 keV, a value approaching the resolution of the magnetic spectrograph used in the previous study of ^{183}Hg decay [16]. Below 100 keV, characteristic x-rays and low energy γ-rays dominate the spectrum.

The detection efficiencies for all detectors (for the Si(Li) detector separately for photons and for electrons) were determined using a dedicated code on the basis of the GEANT4

simulation package [35] with input of the dimensional details of the detectors and their environments. The simulation was validated with known ^{189,187}Hg decays [11, 51], acquired as calibration data as parts of both experiments. Normalisation of the conversion-electron intensities to the γ-ray intensities, obtained from these efficiency curves, was made via the multipolarity of a strong transition (166 keV) and its α_K conversion coefficient calculated using its theoretical value. The multipolarity was established by γ-ray gated electron intensities of subshell lines. This avoids errors due to possible subshell peak contaminant lines. Details are given later. Note, that the low-energy electron and γ-ray lines were both observed in the Si(Li) detector; and with separate efficiency calibrations for detection of both, no geometrical normalisation was necessary.

The fully digital data acquisition system was based on commercial Pixie-16, 14-bit, 250 MHz digitisers [36]. The system was operated in a triggerless mode, i.e., all channels were read out and time stamped independently. The γ–γ coincidence information was reconstructed offline.

4. Experimental results

Previously, the decay of ^{183}Hg has been studied by α-, β-, and γ-decay spectroscopy. The α-decay branch is 12% and details of this decay are described in [37]. Further, details of the ensuing daughter, granddaughter, etc, decays are given in [16]. The β-decay strength has been mapped using total absorption γ-ray spectroscopy (TAS) [38]. Some details of discrete line γ-ray spectroscopy and conversion-electron spectroscopy following β^+/EC decay are described in [16], which also includes some tables of γ–γ coincidence relationships. All of these studies were conducted using mass-separated sources at the ISOLDE [37, 38] and ISOCELE (Orsay, France) [16] facilities.

The half life of ^{183}Hg is 9.4(7)s [39] and the β-decay energy is 6385(12) keV [40]. The β^+/EC decay scheme is distinguished by a large concentration of β-decay strength to states in ^{183}Au in the excitation range 1600–1900 keV. This is clearly mapped in the TAS study [38] and is implicit in some of the assigned γ-ray strength in the study of [16]. In particular, a single state at 1682.30 keV excitation energy in ^{183}Au appears to receive 13^{+15}_{-5}% of the β-decay strength. Using this feature of the decay of ^{183}Hg is a key point in the strategy adopted herein to elucidate the low-energy structure of ^{183}Au via β decay of ^{183}Hg (details of which are given below).

The focus of this study is establishing the energies of the lowest-lying $1h_{9/2}$ and $2f_{7/2}$ intruder states in ^{183}Au relative to the non-intruder $3s_{1/2}$ and $2d_{3/2}$ states. This was carried out in systematic studies in the heavier odd-mass Au isotopes and is summarised in [8, 10, 11]. In these summaries, some details of ^{185}Hg^{m,g} decay to ^{185}Au, taken from an unpublished thesis [12] are presented. Some important details of electric monopole transition strengths in ^{185,187}Au, taken from this thesis, are reported in [13]. These details pointed to serious errors in an earlier study of ^{185}Hg^{m,g} decay to ^{185}Au [41]. Most critical was a failure to identify parity-changing $E1$ transitions, which led to wrong parity assignments for a series of excited states and thus to misinterpretation of the underlying nuclear structure. These errors occurred due to missing of doublets (or even higher multiplets) in measured spectra. Analysis of γ-gated electron spectra and application of a running gates technique solved this problem [8, 11]. These details [8] also pointed to potential errors in the low-energy level scheme of ^{183}Au reported by [16]. However, the ^{185}Au level scheme remains incomplete, since one of the strongest observed low-energy γ-rays is still unassigned [12].

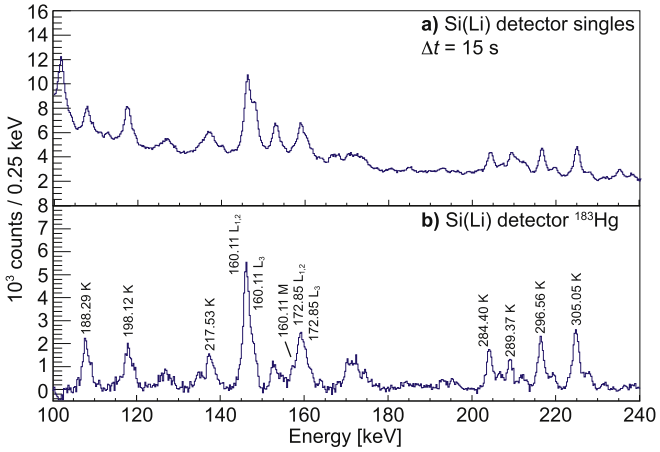

Figure 2. Spectrum of conversion electrons measured with the Si(Li) detector inside the chamber of the HIGH-TATRA system: (a) total singles spectrum and (b) spectrum attributed to the decay of ^{183}Hg deconvoluted using time-stamped data, see the text for details.

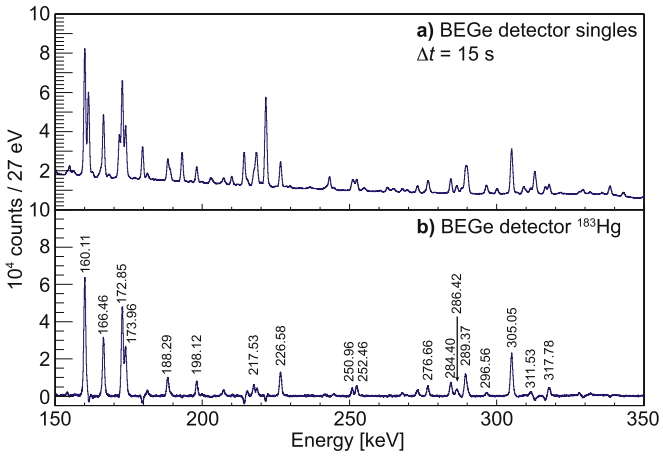

Figure 3. Spectrum of γ-rays measured with the BEGe detector: (a) total singles spectrum and (b) spectrum attributed to the decay of ^{183}Hg deconvoluted using time-stamped data, see the text for details.

The challenge in studying decay schemes in odd-mass nuclei in this mass region is the widely occurring feature of excited states at very low excitation energy (< 50 keV). This has been handled variously with ultra-low energy singles conversion-electron spectroscopy [42, 43] and with low-energy conversion-electron-γ-ray coincidence spectroscopy [8, 13, 14, 44]. We attacked this problem in ^{183}Au [32] using the large number of de-excitation paths of the 1682.30 keV state, strongly populated in β decay (see above), combined with γ-ray spectroscopy employing, in part, the high-energy precision available using a BEGe detector operated at high gain (27 eV/ch). Such data, in combination with γ–γ coincidence spectroscopy, provide a 'map' of low-lying excited states with some use of the

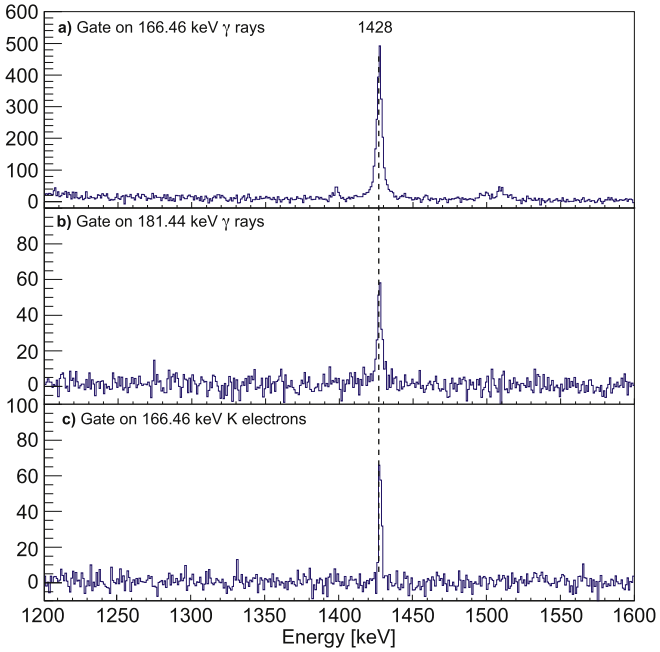

Figure 4. Spectra of γ-rays detected in prompt coincidence with (a) the 166.46 keV γ-rays, (b) 181.44 keV γ-rays, and (c) K electrons from 166.46 keV transition.

Rydberg–Ritz combination principle. This approach to elucidating complex decay schemes, with a high density of states at low energy is described in greater detail in [32].

Figure 2(a) gives a part of the conversion-electron singles spectrum detected with the Si(Li) detector. Since the data from all channels were acquired independently and collected as a stream of the time-stamped data, the events due to the decay of ^{183}Hg isotope could be separated from daughter activities and room background. Spectra corresponding to the early and late parts of the decay curves were produced, normalised and subtracted in such a way that events due to mother and daughter activity were separated. This technique is described in more detail in [32]. An example of such a deconvoluted conversion-electrum spectrum is shown in figure 2(b), where the peaks of daughter activities are subtracted. An example of the γ-ray singles spectrum detected with the BEGe detector is given in figure 3.

For γ–γ coincidence analysis, the data were sorted into different matrices according to detector combinations: BEGe-coaxial, coaxial-BEGe and coaxial–coaxial, where coaxial stands for coaxial Ge detector. The γ-ray-conversion electron coincidences were investigated separately; however only a few coincidence gates with sufficient statistical quality could be produced due to limited running time. The coincidence data were also separated by time tagging so that daughter, grand-daughter, etc, contamination was minimised.

The level scheme of ^{183}Au was constructed on the basis of these coincidences in conjunction with the Rydberg–Ritz combination principle. Figure 4 gives examples of spectra of γ-rays detected in coincidence with either γ-rays or conversion electrons. More coincidence spectra, used to construct level schemes presented here, were published in [32] to support the new level scheme. Figure 5 gives a partial level scheme of low-lying negative-parity states associated with $1h_{9/2}$ and $2f_{7/2}$ intruder configurations that are fed by deexcitation of the 1682.30(2) keV level. Spin assignments are based on the internal conversion coefficients

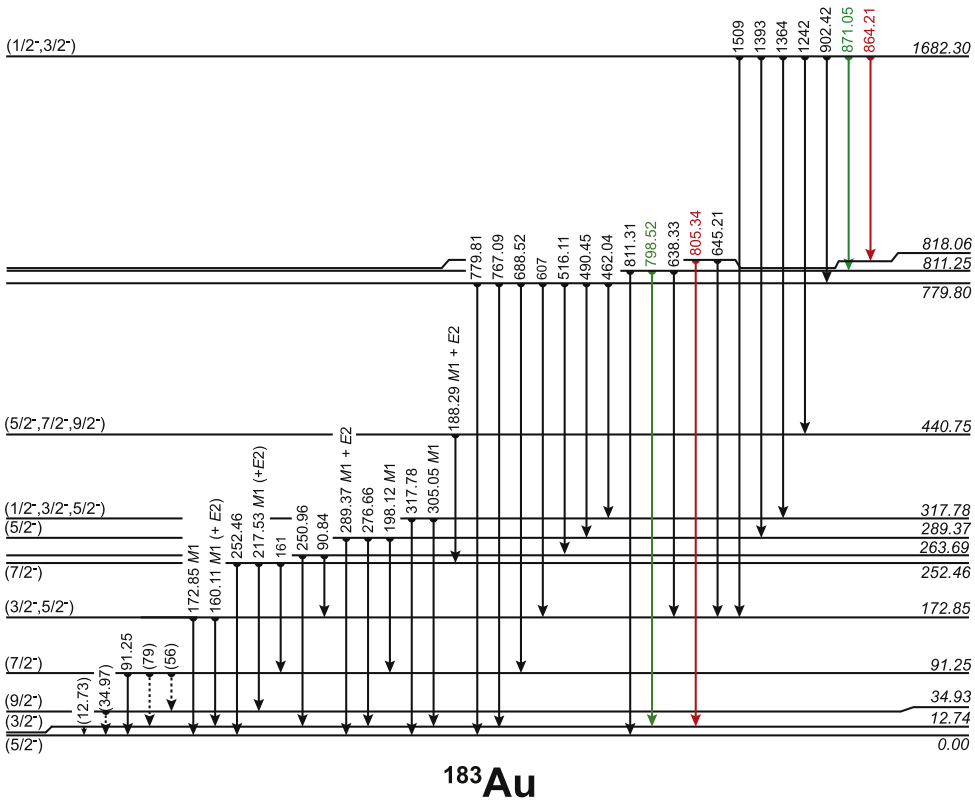

Figure 5. Partial level scheme of low-lying, negative-parity states associated with the $1h_{9/2}$ and $2f_{7/2}$ intruder configurations in the ^{183}Au isotope deduced from the present work. The γ-ray energies of transitions are given. See table 2 for intensities and multipolarities of transitions. Transition energies were determined using the γ-singles spectrum detected with the BEGe detector. Transitions with energies given as integer numbers are either weak, dominated by other γ lines, or their energy exceeds 980 keV, which was the upper limit for the BEGe detector in this experiment, see the text for details. Their location in the scheme is proved by the γ–γ coincidences. All states are populated via the decay of the 1682.30 keV state, see the text for details. Decay paths used for the localisation of the critical 60.73 keV transition connecting intruder and proton–hole states are highlighted in red and green, respectively, see the text for details.

determined in the present study. The excitation energy of the first excited state was determined using energy differences between transitions feeding the ground state and first excited state, arising from deexcitation of the 172.85, 289.37, 317.78, and 779.80 keV states, see figure 5. Further details are given in [32].

The 1682.30(2) keV state is of particular interest since it can be used to determine the energy difference between intruder and non-intruder configurations. Its excitation energy is determined using 871.05(3)-798.52(2) keV and 864.21(3)-805.34(3) keV cascades feeding the first excited state; respective transitions are highlighted in green and red in figure 5. Figure 6 gives the partial level scheme of low-lying positive-parity states associated with the $2d_{3/2}$ and $3s_{1/2}$ proton–hole configurations (together with their decay into negative-parity first-excited and ground states). The cascade of 60.37(1)-173.96(1)-730.93(2)-704.33(2) keV feeding the first-excited state gives the excitation for the initial state of 1682.33(2). This,

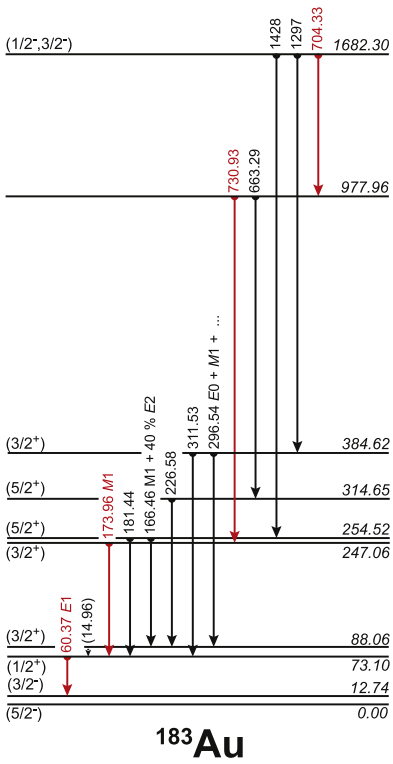

Figure 6. Partial level scheme of low-lying, positive-parity states associated with $3s_{1/2}$ and $2d_{3/2}$ proton–hole configurations in the ^{183}Au isotope deduced from the present work. The γ-ray energies of transitions are given. See table 2 for intensities and multipolarities of transitions. Transition energies were determined using the γ-singles spectrum detected with the BEGe detector. Transitions with energies given as integer numbers are either weak, dominated by other γ lines, or their energy exceeds 980 keV, which was the upper limit for the BEGe detector in this experiment, see the text for details. Decay paths used for the localisation of the critical 60.73 keV transition connecting intruder and proton–hole states are highlighted with red colour, see the text for details.

within experimental uncertainties agrees with the value 1682.30(3) keV determined from the decay scheme of the negative-parity states. Note that all transitions forming this cascade, except the 60.37 keV, are found in coincidence with each other, see figure 7 in [32]. As is demonstrated in the spectrum given in figure 7, the 60.37 keV transition is clearly assigned to the decay of the ^{183}Hg isotope.

To determine the multipolarity of the 60.37 keV transition, the low-energy part of the singles spectrum detected with the Si(Li) detector can be used. Figure 8 gives both the total singles spectrum (panel (a)) and the spectrum with subtracted daughter activities (panel (b)). A strong peak due to 60.37 keV γ-rays together with corresponding L and M conversion electrons is observed. In addition, K_α Au characteristic x-rays and other electron peaks are visible. Using simulated detection efficiencies both for electrons and photons, $\alpha_L = 0.22(4)$ for the 60.37 keV transition is obtained. This unambiguously determines the $E1$ multipolarity for the 60.37 keV transition, see the theoretical value of 0.25 calculated using the BrIcc software [45]. Other multipolarities for the transition are clearly excluded since BrIcc gives an

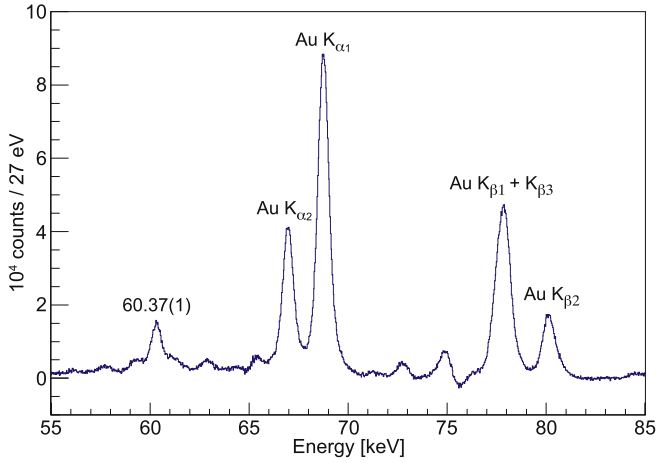

Figure 7. Spectrum of low-energy γ-rays detected with the BEGe detector that are unambiguously attributed to ^{183}Hg decay by deconvolution of time-stamped data, see the text and [32] for details.

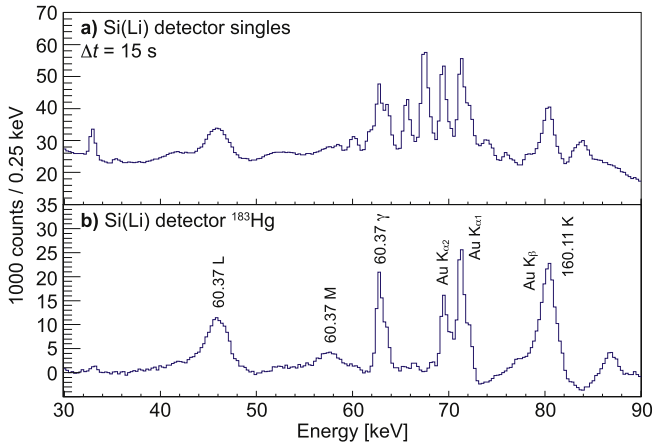

Figure 8. Spectrum of low-energy γ-rays, characteristic x-rays and conversion electrons measured with the Si(Li) detector inside of the chamber of the HIGH-TATRA system: (a) total singles spectrum and (b) spectrum attributed to the decay of ^{183}Hg deconvoluted using time-stamped data, see the text for details. Note that the energy calibration of the spectra shown is for conversion electrons. The calibration for γ-rays and x-rays differs due to the bias on the detector (-500 V), implantation depth into the metallic tape and to dead layer of the Si(Li) detector.

L shell internal conversion coefficient of 4.36 for an $M1$ transition and even larger values for higher multipolarities. The M-shell internal conversion coefficient, $\alpha_M = 0.04(2)$ was deduced for the 60.37 keV transition. This corroborates the $E1$ assignment, see the BrIcc value of 0.05 for $E1$ multipolarity while other multipolarities would have α_M values well above 1. The previous study at the ISOCELE facility [16] assigned the 60.37 keV transition as an 'abnormal' $E1$ transition. Abnormality of the transition was concluded on the basis of an anomalously high α_{L2} value. The measured value was reported to be 0.79, see table 5 in [16],

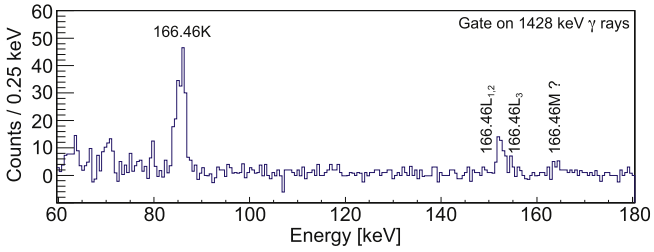

Figure 9. Spectrum of conversion electrons detected in prompt coincidence with the 1428 keV γ-rays.

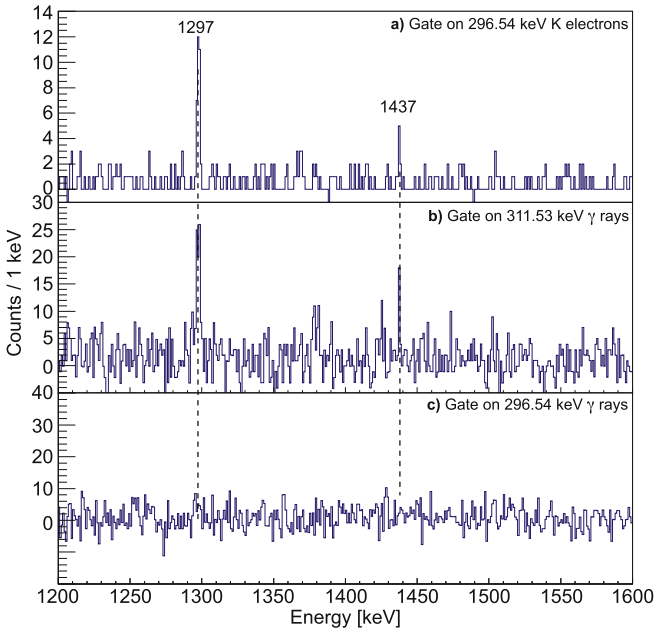

Figure 10. Spectra of γ-rays detected in prompt coincidence with (a) *K* electrons from 296.54 keV transition, (b) the 311.53 keV γ-rays, and (c) 296.54 keV γ-rays.

while the BrIcc code gives 0.0629 for a 60.37 keV *E*1 transition. The Si(Li) detector cannot resolve subshell components of the *L* conversion electrons multiplet. However, if one of the subshell components was anomalously large, the α_L would not agree with the BrIcc calculation, which is not the case for the present data. Therefore, we assign the 60.37 keV as an *E*1 transition with no abnormality.

The 60.37 keV parity-changing *E*1 transition is assigned as a $1/2^+ \rightarrow 3/2^-$ transition, see figure 6. The absence of a transition to the $5/2^-$ ground state supports the spin assignment of $1/2^+$. An analogous *E*1 transition is known in ^{179}Au [28]. Assuming a similar reduced transition probability, a half-life of a few microseconds can be expected for the 73.10 keV state in ^{183}Au. Indeed, no prompt γ–γ coincidences were observed (not even the 511 keV electron–positron annihilation line or characteristic Au K x-rays) with it. Note that the multipolarity is determined from the singles spectrum, which often leads to wrong assignments, but since the initial state is a long-lived isomer, the coincidence technique cannot be

Table 1. Internal conversion coefficients, K/L shell ratios, and multipolarities of transitions determined from present data.

E_γ (keV)	Experimental value	BrIcc ($M1$)	BrIcc ($E2$)	Multipolarity
60.37	$\alpha_L = 0.22(4)$	4.355	37.68	$E1$
	$\alpha_M = 0.04(2)$	1.011	9.782	
160.11	$\alpha_K/\alpha_L = 4.7(18)$	5.99	0.72	$M1$ (+$E2$)
166.46	$\alpha_K/\alpha_L = 3.4(5)$	5.994	0.782	$M1$ + 40(10)% $E2$
	$\alpha_L = 0.24(5)$	0.233	0.338	
172.85	$\alpha_K = 1.25(28)$	1.257	0.242	$M1$
173.96	$\alpha_K = 1.25(28)$	1.234	0.238	$M1$
188.29	$\alpha_K = 0.87(20)$	0.989	0.197	$M1$ (+$E2$)
198.12	$\alpha_K = 0.88(20)$	0.858	0.174	$M1$
217.53	$\alpha_K = 0.54(13)$	0.661	0.138	$M1$ (+$E2$)
284.40	$\alpha_K = 1.21(33)$	0.316	0.071	$E0 + M1 + \cdots$
289.37	$\alpha_K = 0.25(6)$	0.302	0.068	$M1 + E2$
296.54	$\alpha_K = 2.84(74)$	0.282	0.064	$E0 + M1 + \cdots$
305.05	$\alpha_K = 0.26(6)$	0.261	0.060	$M1$
	$\alpha_L = 0.04(1)$	0.043	0.029	

applied. However, the peak density at low energies is not very large, therefore a risk of missing an unresolved doublet is minimal.

Assignment of spins and parities can be made using the spin-parity of the ^{183}Hg ground state (β-decaying state), $J^\pi = 1/2^-$ [46], and that for the ^{183}Au ground state, $J^\pi = 5/2^-$ [47]. The decay energy and half-life of ^{183}Hg provide a log ft value for the decay to the 1682.30 keV excited state in ^{183}Au of $4.9^{+0.5}_{-0.1}$, which suggests a likely spin-parity of $1/2^-$ or $3/2^-$.

Multipolarities of transitions were determined from the present data as follows. The 166.46(1) keV transition shows a strong coincidence (with the 1428 keV transition), see figure 4. The spectrum of conversion electrons detected in a prompt coincidence with the 1428 keV transition is given in figure 9. The ratio of K and L shell conversion coefficients, α_K/α_L is determined to be 3.2(5). Therefore, mixed $M1 + E2$ character of the transition is established since the BrIcc code gives a K/L ratio of 5.75(12) for $E1$, 5.99(12) for $M1$ and 0.782(16) for $E2$ transitions. Higher multipolarities are excluded since they would cause an isomeric character of the transition, which is ruled out by the observation of coincidences. From the above numbers, $M1 + 44(10)\%$ $E2$ is determined. In a previous experiment [16], a 30% $E2$ admixture was deduced (note that no experimental uncertainty was given). A summary of the deduced internal conversion coefficients, K/L shell ratios and multipolarities is given in table 1.

The previous study of ^{183}Au reported two transitions with mixed $E0 + M1 + E2$ multipolarity: 284.4 and 296.7 keV [16]. In the present experiment, both transitions were observed in γ-ray and conversion-electron singles, see figures 2 and 3. More precise energies of 296.54(2) and 284.40(2) keV are determined. Figure 10(a) gives part of the spectrum of γ-rays detected in prompt coincidence with K electrons from the 296.54 keV transition, with 1297 and 1437 keV transitions present. The same transitions are observed in prompt coincidence with the 311.53(2) keV transition, see figure 10(b). The 311.53 keV transition is assigned to the decay of ^{183}Hg, see figure 3. The energy difference between 311.53(2) and 296.54(2) keV transitions is 14.99(3) keV. This compares with the 14.98(2) keV separation

Table 2. Energies, intensities and multipolarities of γ-rays assigned to the decay scheme of ^{183}Au in the present work. The γ-ray intensities are given relative to the 160.11 keV, 172.5 → 12.74 keV transition. Multipolarities of transitions, except for the 60.37 and 166.46 keV, see text for details, are taken from [16].

E_γ (keV)	I_γ	Multipolarity	E_γ (keV)	I_γ	Multipolarity
60.37(1)	440(80)	$E1$	490.45(2)	5(1)	
90.84(3)	14(4)		516.11(1)	32(3)	
91.25(6)	3(1)		583.10(2)	12(2)	
160.11(1)	100(10)	$M1$ (+E2)	607	11(3)	
161(1)	13(3)		638.33(7)	4(2)	
166.46(1)	50(5)	$M1$ + 40(10)% $E2$	645.21(2)	19(2)	
172.85(1)	82(8)	$M1$	663.29(3)	5(1)	
173.96(1)	46(5)	$M1$	688.52(7)	4(2)	
181.44(2)	6(1)		704.33(2)	13(3)	
188.29(1)	19(2)	$M1$ (+E2)	730.93(2)	7(1)	
198.12(1)	19(2)	$M1$	767.09(5)	20(2)	
217.53(1)	14(2)	$M1$ (+$E2$)	779.81(3)	12(2)	
218.30(1)	11(2)		798.52(2)	20(2)	
226.58(1)	29(6)		805.34(3)	16(2)	
250.96(2)	11(2)		811.31(7)	6(2)	
252.46(1)	16(2)		864.21(3)	13(1)	
276.66(2)	20(2)		871.05(3)	18(2)	
284.40(2)	11(2)	$E0$ + $M1$ + ⋯	902.42(8)	17(2)	
286.42(1)	13(2)		1242(1)	7(2)	
289.37(2)	37(4)	$M1$ + $E2$	1297(1)	12(1)	
296.54(2)	6(1)	$E0$ + $M1$ + ⋯	1364(1)	10(1)	
305.05(1)	81(8)	$M1$	1393(1)	20(2)	
311.53(2)	10(2)		1428(1)	83(8)	
317.78(2)	17(2)		1437(1)	16(2)	
462.04(2)	17(2)		1509(1)	32(3)	

between the $1/2^+$ and $3/2^+$ states, determined as a difference between the 181.44(2) and 166.46(1) keV transitions, see figure 6. This defines a new excited state at 384.62(2) keV, see figure 6, which is fed by 1297 and 1437 keV γ-rays emitted from high-lying states 1632.30 keV, 1822 keV (not shown in level schemes), respectively. Interestingly, no coincident γ-rays were observed by gating on the 296.54 keV line, see figure 10(c); but this is probably due to the limited counting statistics of the present data set. This indicates strong conversion of the 296.54 keV transition and thus corroborates the presence of the $E0$ component as suggested in [16]. The $E0$ character of the transition suggests a $3/2^+$ assignment for the 384.62 keV state. Note that no coincidences are observed for the strong, highly converted 284.40(2) keV transition: this is due to the limited counting statistics of the present data set and points to the need for a dedicated, long-duration experiment. Therefore the 284.40(2) keV transition was not placed into the level scheme.

A summary of all transitions assigned to the decay scheme of ^{183}Au in the present work, with their energies, intensities, and some multipolarities is given in table 2. Excited states are summarised together with transitions that de-excite them in table 3.

A set of transitions associated with the $1h_{11/2}$ proton–hole, inverted-spin cascade was reported in a previous study [16]. In the present experiment, these transitions are observed and their energies are precisely determined: 218.30(1), 286.42(1) and 583.10(2) keV. The

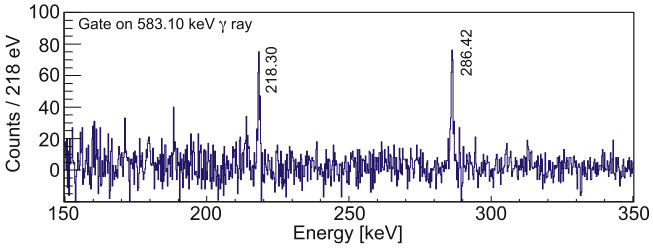

Figure 11. Spectrum of γ-rays detected in prompt coincidence with the 583.10 keV γ-rays.

Table 3. Excited states of ^{183}Au populated in the β^+/EC decay of ^{183}Hg via the 1682.30 keV state and γ-rays assigned to their de-excitation.

Level energy (keV)	J^π	E_γ (keV)
12.74(1)	$(3/2^-)$	
34.93(1)	$(9/2^-)$	
73.10(1)	$(1/2^+)$	60.37(1)
88.06(3)	$(3/2^+)$	
91.25(1)	$(7/2^-)$	91.25(6)
172.85(1)	$(3/2^-, 5/2^-)$	160.11(1),172.85(1)
247.06(2)	$(3/2^+)$	173.96(1)
252.46(1)	$(7/2^-)$	161(1), 217.53(1), 252.46(1)
253.23(1)	$(11/2^-)$	218.30(1)
254.52(2)	$(5/2^+)$	166.46(1), 181.44(2)
263.69(2)		90.84(3), 250.96(2)
289.37(1)	$(5/2^-)$	198.12(1), 276.66(2), 289.37(2)
314.65	$(5/2^+)$	226.58(1)
317.78(1)	$(1/2^-, 3/2^-, 5/2^-)$	305.05(1), 317.78(2)
384.62(2)	$(3/2^+)$	296.54(2), 311.53(2)
440.75(1)	$(5/2^-, 7/2^-, 9/2^-)$	188.29(1)
539.65(2)	$(7/2^-)$	286.42(1)
779.80(2)		462.04(2), 490.45(2), 516.11(1), 607(1), 688.52(7), 767.09(5), 779.81(3),
811.25(2)		811.31(7), 798.52(2), 638.33(7)
818.06(2)		645.21(2), 805.34(3)
977.96(2)		663.29(3), 730.93(2)
1122.75(3)	$(3/2^-)$	583.10(2)
1682.30(2)	$(1/2^-, 3/2^-)$	704.33(2), 864.21(3), 871.05(3), 902.42(8), 1242(1), 1297(1), 1364(1), 1393(1), 1428(1), 1509(1)

coincidence relationships of these transitions are confirmed, see figures 11 and 12. In odd-Au isotopes in the vicinity of the $N = 104$ midshell, the $11/2^-$ band head associated with the $1h_{11/2}$ configuration is known to decay to the $9/2^-$ proton-intruder state via a retarded $M1$ transition [8]. Therefore, we propose the partial level scheme depicted in figure 13. New

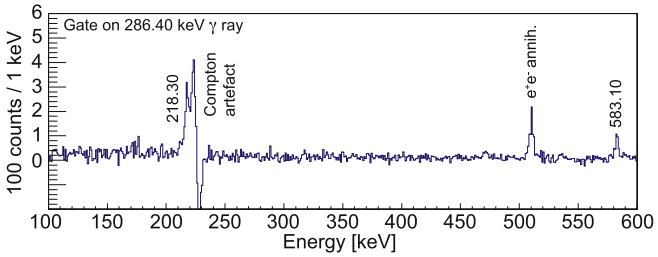

Figure 12. Spectrum of γ-rays detected in prompt coincidence with the 286.40 keV γ-rays. The structure denoted as 'Compton artefact' is due to scattering of 511 keV electron–positron annihilation quanta between two germanium detectors.

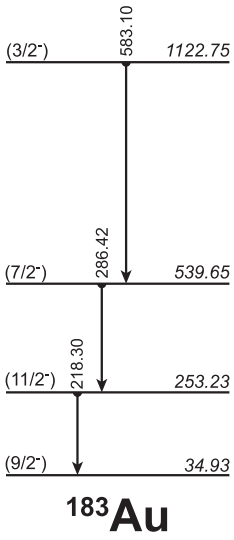

Figure 13. Partial level scheme of negative-parity states associated with the $1h_{11/2}$ proton–hole configuration in the ^{183}Au isotope deduced from the present work. The $9/2^-$ state is due to the $1h_{9/2}$ intruder configuration.

excited states with energies 253.23(1), 539.65(2), and 1122.75(3) keV are identified. Spin assignments are based on a comparison with known systematics, see discussion below.

5. Discussion

The key outcome of this work, which is depicted in figure 14, is the elucidation of the intruder states relative to the normal states in ^{183}Au. This suggests that the 'parabolic' trend, widely observed to be characteristic of the intruder states [3], has a minimum in ^{183}Au, i.e., at the $N = 104$ the mid-neutron shell. It is also interesting to note that the isotopes where the intruder state becomes the ground state correspond to nuclei for which the mean-square charge radius has been observed to depart suddenly from the trend set by the heavier isotopes. In particular, ^{187}Au has both a normal ground state and a normal $\delta\langle r^2\rangle$, while ^{185}Au has an intruder ground state and a large $\delta\langle r^2\rangle$ [48, 49]. Further, it has been predicted that the nuclear

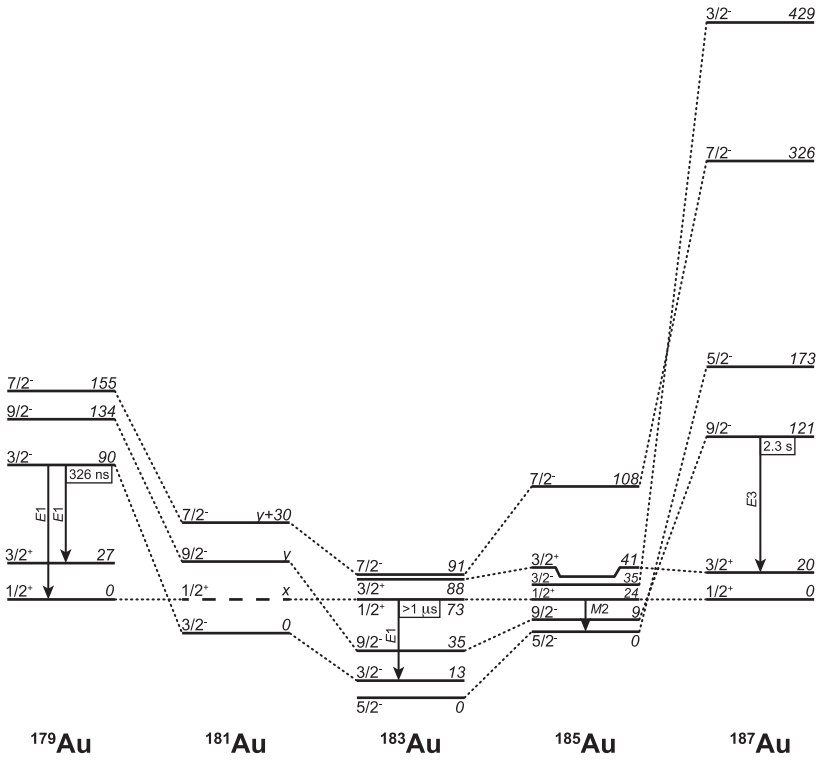

Figure 14. Systematics of $9/2^-$, $7/2^-$, $3/2^-$, and $1/2^-$ states associated with the $1h_{9/2}$ and $2f_{7/2}$ intruder configurations and $1/2^+$, and $3/2^+$ states of $2d_{3/2}$ and $3s_{1/2}$ proton–hole configurations in odd-Au isotopes. Important parity-changing transitions that are connecting these intruder and proton–hole configurations are indicated. Note that the half life of the $1/2^+$, 24 keV state in ^{185}Au is unknown and only inadequate data [50] are available for the ^{181}Au isotope. The data are taken from this work and from [8, 11, 28, 51].

mean-square charge radii will return to their original trend beyond ^{181}Au (see figure 31 in [15]), where the normal configuration becomes the ground state again (see ^{179}Au in figure 14 and [28]).

A number of other key features of ^{183}Au emerge. First, the energy separation of 56.32 keV between the $9/2^-$, 34.93 keV and the $7/2^-$, 91.25 keV states, based on the present work, matches the in-beam high-spin γ-ray study [22, 23] of ^{183}Au which placed these two states at a separation of 56.2 keV. Second, the positive-parity states in ^{183}Au closely match those in ^{185}Au, see figure 16. We also note that a set of states associated with the $1h_{11/2}$ configuration was suggested by [16]: this set of states can be shifted upwards in energy, see figure 13. This closely matches the $1h_{11/2}$ inverted-spin band structure in ^{185}Au and the heavier odd-mass Au isotopes, see the systematics given in figure 15. For extensive systematics, see [5].

The present work points to a number of incorrect features in the previous study of the $^{183}\text{Hg} \rightarrow {}^{183}$Au decay scheme [16]. A major disagreement is the assignment of a level at 12.3 keV with a spin-parity of $9/2^-$ [16]. The basis for this assignment was a coincidence-based cascade of γ-rays with energies of 250.9, 516.3, and 902.2 keV from a 1682.1 keV

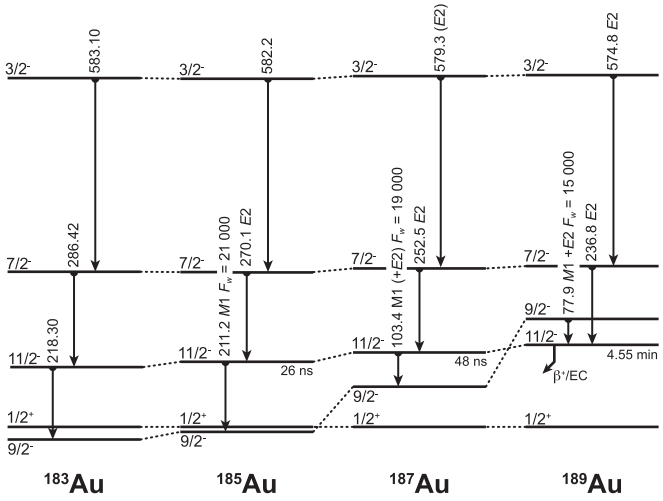

Figure 15. Systematics of negative-parity states associated with the $1h_{11/2}$ proton–hole configuration in odd-Au isotopes. Data are taken from this work and from [8, 11, 51].

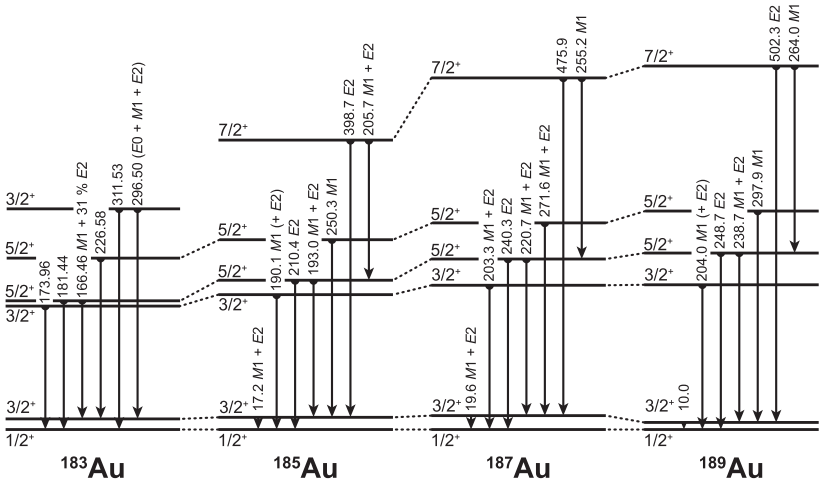

Figure 16. The systematics of the bands built on the low-lying, low-spin, positive-parity states of $2d_{3/2}$ and $3s_{1/2}$ configurations in odd-Au isotopes. Data are taken from this work and from [8, 11].

level. Support for the 12.3 keV level was argued to come from a pair of γ-rays with energies of 284.4, 296.7 keV (based on their energy difference of 12.3 keV). We note that the energy sum of the cascade yields 12.8, not 12.3 keV. The energies for this cascade in the present work are 250.96, 516.11, and 902.42 keV from the 1682.30 keV level, i.e., terminating in a level at 12.81 keV, see the level in the present scheme at 12.74 keV. Note that the uncertainty in the energy of the 902.42 keV γ-ray is 0.08 keV, consistent with the cascade ending in the 12.74 keV level: this illustrates the motivation for conducting these experiments with high energy gain.

We observe γ-ray lines at 284.40 and 296.54 keV, i.e., an energy difference of 12.10 keV. However, the γ-ray gated electron data do not support these two γ-rays originating from the same level. Indeed, as shown in figure 6, we assign the 296.54 keV transition in the scheme (384.62 keV $\rightarrow$ 88.06 keV) in a very different location to that presented in [16]. This location depends on coincidences between the 1297 keV γ-ray and 296.54 K electrons (and 311.53 keV γ-rays). The statistical quality of the present data sets are insufficient to make a reliable assignment of a 284.40 keV transition in the scheme; but this will be critical in the ongoing exploration of the structure of ^{183}Au because of its confirmed $E0$ character (see table 2).

Other aspects of the earlier study of the ^{183}Hg $\rightarrow$ ^{183}Au decay scheme [16] that are clarified by the present study are the completion of the systematics of the low-energy positive-parity states: this is depicted in figure 16. The key to the success of the present work, with respect to this feature of the scheme, is the coincidence-supported Rydberg–Ritz energy combinations, as detailed in [32].

Theoretical description of shape coexistence in the odd-Au isotopes is in a satisfactory state: the parabolic nature of the intruder state energies has been explained (see figure 4 in [3]). Details of the multiple shape-coexisting bands in ^{187}Au have been explored in [9–11]. These studies are an extension of earlier work [52].

The detailed spectroscopic information for ^{183}Au obtained in the present study indicates that particle-core coupling with respect to both the ^{182}Pt and ^{184}Hg cores has the potential to further our knowledge of the shapes of these nuclei. The validity of this claim can be inferred from the systematics established herein, combined with the detailed theoretical analyses, e.g., of ^{187}Au [10, 11] and ^{189}Au [53].

The emerging challenge is the exploration of the shape-coexisting structures in the neighbouring $^{A+1}$Hg and $^{A-1}$Pt cores. At present, there is the very limited view obtained through a few excited states that decay by $E0$ transitions in ^{185,187}Au [10, 11, 13], and now the first hint of such structures in ^{183}Au. This brings a focus to ^{185}Au and the potential offered by both high-spin and low-spin β decays of ^{185}Hg. Some further details on such a study are made in the summary remarks.

6. Summary

In summary, the present investigation of excited states in ^{183}Au, via γ-ray and conversion-electron spectroscopy following the β^+/EC decay of ^{183}Hg, employed a BEGe detector operated at an high gain (27 eV/ch). In consequence, with time-tagged data acquisition in singles and coincidence mode, it has been possible to isolate key decay branches in the decay of ^{183}Hg to ^{183}Au (from the many daughter, grand-daughter, ... decays). In particular, we make use of a specific feature of the decay of ^{183}Hg to ^{183}Au, namely the concentration of a significant fraction of the β-decay strength in the feeding of an excited state in ^{183}Au at 1682.30 keV. This state acts as a 'feeder' state with multiple decay paths to the low-lying states. These decay paths can be placed into a unique pattern using coincidence relationships and Rydberg–Ritz combinations (at the $\pm$30 eV level of precision).

This establishes, for the first time, a reliable identification of the excitation energy of the $1h_{9/2}$ and $2f_{7/2}$ intruder states relative to the non-intruder $3s_{1/2}$ and $2d_{3/2}$ states. A significant number of these excited states must decay by very low-energy, highly converted transitions and so cannot be observed in γ-ray spectroscopy. The pattern of these coexisting states closely matches that in ^{185}Au and the heavier odd-mass Au isotopes. The pattern also matches

limited but critical data for ^{179}Au [28]. So far, there are no data available to address the issue of the relative energies of coexisting states in ^{181}Au.

Within the comprehensive study of ^{187}Au [11], the calculations on the basis of the particle-triaxial-rotor-model [54] using a Woods–Saxon potential for the deformed mean field were performed. Satisfactory agreement between calculations and experimental was obtained, suggesting the weakly prolate triaxial deformation ($\beta_2 = 0.15$and $\gamma = 45°$) for the the non-intruder $3s_{1/2}$ and $2d_{3/2}$ states. The similar pattern of excited states of the $3s_{1/2}$ and $2d_{3/2}$ configuration in ^{183,185}Au, see figure 16, suggests very similar weak triaxial deformation also in lighter isotopes. Similarly, the $1h_{11/2}$ states were found to have weakly deformed triaxial shape ($\beta_2 = 0.15$and $\gamma = 32°$) in ^{187}Au and this appears to not change also in lighter Au isotopes, see figure 15. Dedicated in-beam γ-ray study of the ^{183}Au [23] revealed rotational bands based on the $1h_{9/2}$ and $2f_{7/2}$ intruder states, which indicate strong deformation. These strongly deformed intruder states coexist with weakly deformed triaxial states discussed above.

A comparison of the states below 300 keV in ^{183}Au, established in the present work, with states in ^{179}Au [28] and ^{185,187}Au [8] suggests that ^{183}Au, i.e., $N = 104$ (the middle of the neutron shell) is the location of the minimum of the $1h_{9/2}$ intruder state 'parabola'.

The HIGH-TATRA system has proved its potential to detect γ-rays and conversion electrons simultaneously and with good energy resolution. These techniques were successfully used to study the lowest excited states in ^{183}Au. However, to establish a complete picture of shape coexistence in odd-Au isotopes more experiments will be needed. First of all, a high-statistics study of the ^{183}Au isotope is essential. This will locate a second observed $E0$ transition and will extend the systematics of multiple-coexisting structures. The nucleus ^{185}Au also needs more detailed study than was achieved in [12], since key information, such as the location of important strong γ lines, is still missing. Such an experiment will involve the resonant laser ionisation technique to separate high- and low-spin isomers in ^{185}Hg. Later, a study of the ^{181}Au isotope with so-far almost unknown low-spin structure will follow. With a future intensity upgrade of the ISOLDE facility, the study of ^{179}Hg decay will also become feasible.

Acknowledgments

The authors express their gratitude to the ISOLDE collaboration, the ISOLDE machine operators, and the CERN radioprotection team for excellent support. Special thanks go to the ISOLDE physics coordinators Magdalena Kowalska and Karl Johnston for their help. Very special thanks go to my wife Janka and daughters Stanka and Katka for their love, massive support, patience, and understanding. Fruitful discussions with Tibor Kibédi and Ed Zganjar are highly acknowledged. This work was supported by the Ministry of Education, Science, Research and Sport of the Slovak Republic, the Slovak Research and Development Agency under contract No. APVV-15-0225, by Slovak grant agency VEGA (contract nr. 2/0129/17), by the United Kingdom Science and Technology Facilities Council (STFC) by EU Seventh Framework through ENSAR No. 506065, by IUAP—Belgian Science Policy (BRix network P7/12), by GOA 10/010 from KU Leuven, and by FWO Flanders. T E Cocolios was supported by STFC Ernest Rutherford Fellowship No. ST/J004189/1. PMP gratefully acknowledges the grant received from Programme SASPRO No. 0098/01/01, which is co-funded by the European Commission under the scheme 'Co-financing of regional, national and international programmes (COFUND)', which is part of the Marie Curie Action of the EU 7th Framework Programme, under Grant Agreement No. REA 609427: SASPRO/Mobility Programme of the Slovak Academy of Sciences.

References

[1] Heyde K, Van Isacker P, Waroquier M, Wood J L and Meyer R A 1983 *Phys. Rep.* **102** 291
[2] Wood J L, Heyde K, Nazarewicz W, Huyse M and Van Duppen P 1992 *Phys. Rep.* **215** 101
[3] Heyde K and Wood J L 2011 *Rev. Mod. Phys.* **83** 1467
[4] 2016 Focus on shape coexistence in nuclei *J. Phys. G: Nucl. Part. Phys.* **43** (http://iopscience.iop.org/journal/0954-3899/page/Focus%20on%20shape%20coexistence%20in%20nuclei)
[5] Zganjar E F *et al* 1975 *Phys. Lett.* B **58** 159
[6] Berg V *et al* 1975 *Nucl. Phys.* A **244** 462
[7] Bourgeois C *et al* 1978 *Nucl. Phys.* A **295** 424
[8] Kortelahti M O *et al* 1988 *J. Phys. G: Nucl. Phys.* **14** 1361
[9] Rupnik D 1994 *PhD Thesis* Louisiana State University, Baton Rouge, LA, USA
[10] Rupnik D *et al* 1997 *Phys. Rev.* C **51** R2867
[11] Rupnik D *et al* 1998 *Phys. Rev.* C **58** 771
[12] Papanicolopoulos C D 1987 *PhD Thesis* Georgia Institute of Technology, Atlanta, GA, USA
[13] Papanicolopoulos C D, Grimm M A, Wood J L *et al* 1988 *Z. Phys. A: At. Nucl.* **330** 371
[14] Zganjar E F *et al* 2016 *J. Phys. G: Nucl. Part. Phys.* **43** 024013
[15] Wood J L *et al* 1999 *Nucl. Phys.* A **651** 323
[16] Macias-Marques M I *et al* 1984 *Nucl. Phys.* A **427** 205
[17] Kahler A C *et al* 1978 *Phys. Lett.* **72B** 443
[18] Desthuilliers M G *et al* 1979 *Nucl. Phys.* A **313** 221
[19] Larabee A J *et al* 1986 *Phys. Lett.* B **169** 21
[20] Joshi P *et al* 2004 *Phys. Rev.* C **69** 044304
[21] Joshi P *et al* 2002 *Phys. Rev.* C **66** 044306
[22] Song L T *et al* 2005 *Phys.Rev.* C **71** 017302
[23] Mueller W F *et al* 1999 *Phys. Rev.* C **59** 2009
[24] Soramel F *et al* 1999 *Eur. Phys. J.* A **4** 17
[25] Mueller W F *et al* 2004 *Phys. Rev.* C **69** 064315
[26] Kondev F G *et al* 2001 *Phys. Lett.* **512B** 268
[27] Poli G N *et al* 1999 *Phys. Rev.* C **59** R2979
[28] Venhart M *et al* 2011 *Phys. Lett.* B **695** 82
[29] Harkness-Brennan L J *et al* 2014 *Nucl. Instrum. Methods Phys. Res.* A **760** 28
[30] Stanja J *et al* 2013 *Phys. Rev.* C **88** 054304
[31] Ritz W 1908 *Astrophys. J.* **28** 237
[32] Venhart M *et al* 2017 *Nucl. Instrum. Methods Phys. Res. Sect.* A **849** 112
[33] Kugler E *et al* 2000 *Hyperfine Int.* **129** 23
[34] Matoušek V *et al* 2016 *Nucl. Instrum. Methods Phys. Res.* A **812** 118
[35] Allison J *et al* 2006 *IEEE Trans. Nucl. Sci.* **53** 270
[36] Tan H *et al* 2008 *Nuclear Science Symp. Conf. Record, NSS '08, IEEE* p 3196
[37] Hagberg E *et al* 1979 *Nucl. Phys.* A **318** 29
[38] Hørnshoj P *et al* 1975 *Nucl. Phys.* A **239** 15
[39] Baglin C M 2000 *Nucl. Data Sheets* **91** 117
[40] Wang M *et al* 2012 *Chin. Phys.* C **36** 1603
[41] Bourgeois C *et al* 1982 *Nucl. Phys.* A **286** 308
[42] Roussière B *et al* 1998 *Nucl. Phys.* A **643** 331
[43] Roussière B *et al* 2000 *Hyperfine Int.* **129** 119
[44] Jentoft-Nilsen K *et al* 1999 *Phys. Rev.* C **59** 2422
[45] Kibédi T *et al* 2008 *Nucl. Instrum. Methods Phys. Res.* A **589** 202
[46] Bonn J *et al* 1976 *Z. Phys. A: At. Nucl.* **276** 203
[47] Krönert U, Becker S, Bollen G *et al* 1988 *Z. Phys. A: At. Nucl.* **331** 521
[48] Wallmeroth K *et al* 1987 *Phys. Rev. Lett.* **58** 1516
[49] Wallmeroth K *et al* 1987 *Nucl. Phys.* A **493** 224
[50] Sauvage J *et al* 1992 *Nucl. Phys.* A **540** 83
[51] Wood J L *et al* 1996 *Nucl. Phys.* A **600** 283
[52] Nazarewicz W *et al* 1990 *Nucl. Phys.* A **512** 61
[53] Wood J L *et al* 1976 *Phys. Rev.* C **14** 682
[54] Larsson S E, Leander G A and Ragnarsson I 1978 *Nucl. Phys.* A **307** 189